Contrasting LH-HH subband splitting of strained quantum wells grown along [001] and [113] directions

D. F. Cesar,[1] M. D. Teodoro,[1] H. Tsuzuki,[1] V. Lopez-Richard,[1] G. E. Marques,[1] J. P. Rino,[1] S. A. Lourenço,[2] E. Marega, Jr.,[3] I. F. L. Dias,[4] J. L. Duarte,[4] P. P. González-Borrero,[5] and G. J. Salamo[6]

[1]*Departamento de Física, Universidade Federal de São Carlos, 13560-905 São Carlos, SP, Brazil*

[2]*Departamento de Física, Universidade Federal de Uberlândia, Uberlândia, MG, Brazil*

[3]*Instituto de Física, Universidade de São Paulo, São Carlos, SP, Brazil*

[4]*Universidade Estadual de Londrina, 86051-970 Londrina, PR, Brazil*

[5]*Universidade Estadual do Centro Oeste, 85040-080 Guarapuava, PR, Brazil*

[6]*Department of Physics, University of Arkansas, 226 Physics Building, 72701 Fayetteville, AR, Brazil*

(Received 23 December 2009; revised manuscript received 8 April 2010; published 1 June 2010)

Contrasting responses for the temperature tuning of the electronic structure in semiconductor quantum wells are discussed for heterolayered structures grown along [001] and [113] directions. The temperature affects the strain modulation of the deformation potentials and the effective optical gap is tuned along with the intersubband splitting in the valence band. A multiband theoretical model accounts for the characterization of the electronic structure, highlighting the main qualitative and quantitative differences between the two systems under study. The microscopic source of strain fields and the detailed mapping of their distribution are provided by a simulation using classical molecular-dynamics technics.

DOI: 10.1103/PhysRevB.81.233301 PACS number(s): 78.55.Cr, 78.67.De, 78.20.Bh

Semiconductor interfaces have played a fundamental role since the beginning of the development of semiconductor devices based on Si, II-VI and III-V heterostructure technologies. In 1980s, much attention was focused on GaAs/AlGaAs heterolayered structures grown on GaAs (100) planes as promising candidates to replace the Si/SiO_2 interface. Even with extremely smooth surfaces, the performance of GaAs/AlGaAs heterointerfaces used in devices is affected by deep defects occurring on the barriers. The motivation for growth of GaAs off-(001) planes results from the high concentration of nonreactive empty single dangling bonds which reduces the overall background incorporation of impurities, particularly carbon, and ensures a relatively low background of impurities that compensates the deep defects on AlGaAs barriers.[1]

The electronic, optical, and transport properties in semiconductors nanostructures, and quantum wells (QWs), in particular, are strongly dependent on the substrate orientation due to strain effects and valence effective-mass anisotropy[2–5] and enhanced in the presence of anisotropic confinement. When QWs are grown on nonconventional planes, these effects are drastically altered.[6] Among all the singular, vicinal, or high index surfaces, the (113) plane presents unique features which have attracted attention during the last decades.[7] In this work, we report on a peculiar anisotropy of GaAs/AlGaAs heterolayered structures that leads to opposite responses to temperature of the optical emissions. Such a behavior has been experimentally detected in the photoluminescence (PL) and reproduced by electronic-structure calculation in conjunction with molecular-dynamics simulations, which revealed the atomic-scale nature of these interface effects. The unique low-dimensional properties of layered structures have been the topic for basic research and device applications in the past,[8,9] although interesting behaviors still appear. We explored the effects of strain using temperature variation. This was accomplished by determining the difference between light-hole (LH) and heavy-hole (HH) energy peaks ($E_1^{LH}-E_1^{HH}$), obtained from PL measurements within the temperature range, 12 to 300 K.

Analyzing PL spectra we see that, for structures grown along [113] direction, the $|E_1^{LH}-E_1^{HH}|$ splitting is enhanced and increases with temperature. On the other hand, for growth along the [001] direction, the $|E_1^{LH}-E_1^{HH}|$ splitting is less pronounced and shows a contrasting slope with respect to the [113] direction. To investigate theoretically the expected temperature dependence of $|E_1^{LH}-E_1^{HH}|$ splitting, we performed a 4×4 $\mathbf{k}\cdot\mathbf{p}$ electronic-structure calculation where strain effects are included. Our model provides a general description of hole subbands dependences with strain and temperature for both [001] and [113] directions. For the [113] orientation, analytical expressions are deduced correlating the deformation tensor components.

GaAs/AlGaAs multi-QWs (MQWs) were grown by molecular-beam epitaxy on semi-insulating GaAs (001) and (113)A substrates. The QWs and barriers thickness as well as Al concentrations were determined by high resolution x-ray diffraction (HRXRD). The sample structural parameters and the conditions for the PL measurements are described in Ref. 10. The PL spectra of the MQWs at various temperatures are shown in Fig. 1 for samples grown along (a) [001] and (b) [113] directions. At low temperatures, both samples display a single peak while above 90 K, a shoulder appears with increasing intensity as the temperature rises. The nature of these transitions was determined by the multiband calculation that confirmed their coincidence with HH and LH recombinations.[11] The characterization of the relative positions of these two peaks with temperature allows a detailed analysis of the effects associated to confinement and built-in strains.[12] Figure 1(c) shows the temperature dependence of the difference between LH and HH energy peaks, $|E_1^{LH}-E_1^{HH}|$, for samples grown along [001] and [113] directions. The experimental data shown in Fig. 1(c) were obtained

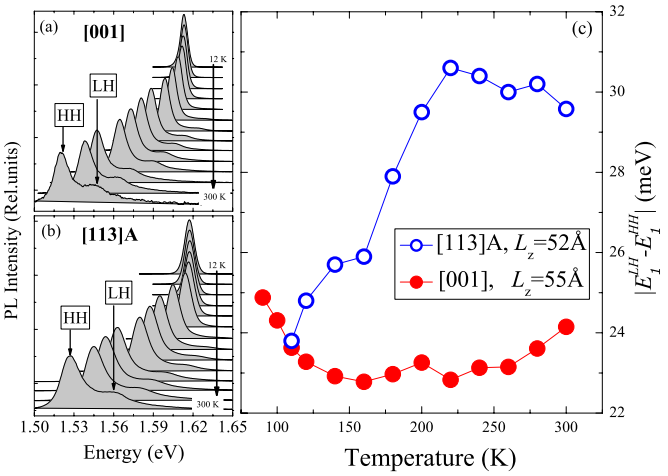

FIG. 1. (Color online) PL spectra for different temperatures of the (a) 55 Å $Al_{0.36}Ga_{0.64}As$ MQWs grown along [001] direction and (b) 52 Å $Al_{0.33}Ga_{0.67}As$ MQWs along [113] direction. The excitation intensity was 16 W/cm^2. (c) Temperature dependence of the difference between LH and HH energy peaks, $|E_1^{LH}-E_1^{HH}|$, for [001] and [113] directions.

from a Lorentzian fitting of PL spectra, displayed in Figs. 1(a) and 1(b), respectively.

Given the anisotropic nature of the valence-band effective mass and the strain-induced effects, the electronic structure of the systems under consideration will respond to the crystallographic orientation of the interfaces. For the relative position between valence subbands, a multiband calculation was set in order to account for the effects associated to confinement, mass anisotropy, and strain within the same theoretical framework.[13–15] The system is described by a 4×4 $\mathbf{k}\cdot\mathbf{p}$ Hamiltonian given by

$$\mathcal{H}=\begin{bmatrix} P^+ & -S & R & 0 \\ & P^- & 0 & R \\ & & P^- & S \\ & & & P^+ \end{bmatrix}, \tag{1}$$

where $P^{\pm}$, S, and R must be defined for each $[hhk]$ direction. We will introduce the subindex "L" in the matrix elements above to identify them as Luttinger matrix elements and "BP" to account for the elements in the Bir-Pikus Hamiltonian,[16] that describes the strain corrections. Although the strain Hamiltonian for systems grown along directions [001], [111], and [112] have been profusely studied, no explicit reference can be found for systems grown along the direction [113] that could help to describe the anomalous behavior observed in the experiment. Thus, we should provide the explicit dependence of the Luttinger Hamiltonian and strain corrections for this case in order to discuss the nature of each contribution. The matrix elements for the system grown along the [001] direction can be found, for instance, in Ref. 13. Yet, for the growth along [113] direction, no explicit expressions were found in literature and we are giving them as

$$P_L^{\pm}=\frac{1}{2}(\gamma_1\pm\gamma_{57,64})k_{\parallel}^2+\frac{1}{2}(\gamma_1\mp\gamma_{57,64})k_z^2 \pm\frac{24}{121}\gamma_\delta[-6\sqrt{2}k_xk_y+(k_x^2-k_y^2)], \tag{2}$$

$$R_L=-\frac{\sqrt{3}}{2}\gamma_{70,51}k_-^2+\frac{2\sqrt{3}}{121}\gamma_\delta[12\sqrt{2}k_-k_z-4(k_{\parallel}^2+2k_z^2-21\sqrt{2}k_+k_z-24k_+^2)], \tag{3}$$

$$S_L=\sqrt{3}\gamma_{83,38}k_-k_z+\frac{\sqrt{3}}{121}\gamma_\delta[-12\sqrt{2}(k_{\parallel}^2-4k_z^2+k_-^2)-32k_+k_z+21\sqrt{2}k_+^2]. \tag{4}$$

The following notation has been used for linear combinations of Luttinger parameters $(\gamma_1,\gamma_2,\gamma_3)$: $\gamma_\delta=\frac{1}{2}(\gamma_3-\gamma_2)$, $\bar{\gamma}=\frac{1}{2}(\gamma_3+\gamma_2)$, $\gamma_s=\frac{1}{5}(3\gamma_3+2\gamma_2)$, and $\gamma_{n,p}=\frac{n\gamma_3+p\gamma_2}{n+p}$. We have also used: $k^2=k_x^2+k_y^2+k_z^2$, $k_{\parallel}^2=k_x^2+k_y^2$, and $k_{\pm}=k_x\pm ik_y$. The matrix elements of the Bir-Pikus Hamiltonian for the system grown along [113] direction can be written as

$$P_{BP}^{\pm}=\frac{1}{2}(2\varepsilon_{\parallel}+\varepsilon_{\perp})\beta_1\pm(\varepsilon_{\parallel}-\varepsilon_{\perp})\beta_{57,64}\mp\frac{144\sqrt{2}}{121}\beta_\delta\varepsilon_{13}, \tag{5}$$

$$R_{BP}=-2\sqrt{3}[9\sqrt{2}\varepsilon_{13}+8(\varepsilon_{\parallel}-\varepsilon_{\perp})]\beta_\delta, \tag{6}$$

$$S_{BP}=\sqrt{3}\beta_{67,54}\varepsilon_{13}-\frac{48\sqrt{6}}{121}(\varepsilon_{\parallel}-\varepsilon_{\perp})\beta_\delta. \tag{7}$$

Here, the combination of parameters are $\beta_\delta=\frac{1}{2}(\beta_3-\beta_2)$, $\bar{\beta}=\frac{1}{2}(\beta_3+\beta_2)$, $\beta_s=\frac{1}{5}(3\beta_3+2\beta_2)$, and $\beta_{n,p}=\frac{n\beta_3+p\beta_2}{n+p}$, where $\beta_1=2a$, $\beta_2=b$, $\beta_3=d/\sqrt{3}$ and a, b, and d are deformation potentials.

The GaAs and AlAs lattices have very close lattice parameters,[17] yet strain fields are produced at their interfaces. In order to quantify the stress in the GaAs/AlAs interface, we performed molecular-dynamics simulations based on an effective interatomic potential. The many-body interatomic potentials for both materials were based on the modeling reported in Ref. 18 in which two- and three-body interactions were considered. The parameters in the effective interatomic potential, for both semiconductors, were chosen in order to reproduce cohesive energy, bulk modulus, and C_{11} elastic constant at experimental densities. The interaction between atoms at interface is obtained by interpolation between AlAs and GaAs potentials as specified in Ref. 18 by considering the local chemical environment.[18,19]

Two interfaces were prepared creating a single quantum well, AlAs/GaAs/AlAs, at different crystallographic orientations. A total of 72 128 atoms is used in one simulation, where the single well has the dimension of $39.56\times39.56\times1039.56$ $Å^3$ along x, y, and z directions which are parallel to the [100], [010], and [001] crystallographic directions, respectively. In this case, the well has a thickness of 56.2 Å and the barriers 491.68 Å. The other simulation was pre-

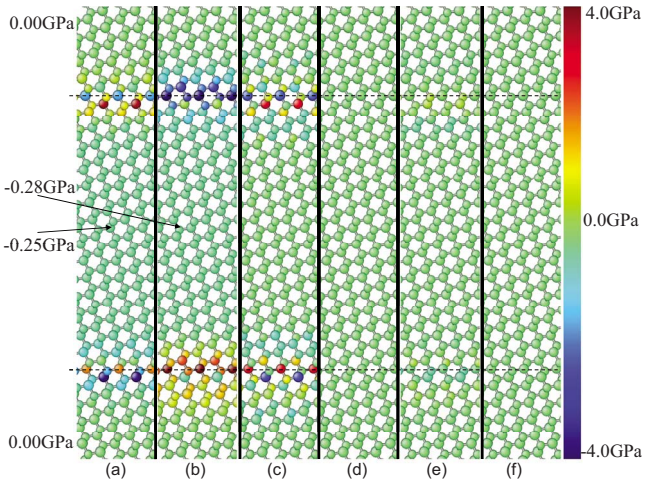

FIG. 2. (Color online) Visualization of the (113) wells regions on a $(\bar{1}10)$ plane with different components of the stress tensor. (a) $\mathcal{T}_{11}$ with central well region around −0.28 GPa. (b) $\mathcal{T}_{22}$ with central well region around −0.25 GPa. (c) $\mathcal{T}_{33}$. (d) $\mathcal{T}_{12}$. (e) $\mathcal{T}_{13}$. (f) $\mathcal{T}_{23}$.

pared with $39.76\times39.96\times1049.46$ Å^3 with x, y, and z parallel to $[33\bar{2}]$, $[\bar{1}10]$, and [113], respectively, using a total of 73 920 atoms. The well is 56.0 Å thick and the barriers, 496.73 Å. Periodic boundary conditions were applied in all directions. Before any analysis, the whole system was allowed to relax in order to have zero pressure. For each case studied, the system was very well thermalized at temperature close to 0 K. From this configuration, the distribution of local stress was calculated using the algorithm supplied in Ref. 20.

Among all 36 stress tensor components, $\mathcal{T}_{11}$, $\mathcal{T}_{22}$, $\mathcal{T}_{33}$, $\mathcal{T}_{12}$, $\mathcal{T}_{13}$, and $\mathcal{T}_{23}$ are shown in Fig. 2. It shows the calculated stress tensors with a view of (311) wells on a $(\bar{1}10)$ plane. Observe that the stress at the interface can be as strong as ±4 GPa while in the central region of the well is compressive with $\mathcal{T}_{11}\sim-0.25$ GPa and $\mathcal{T}_{22}\sim-0.28$ GPa. Also note that the stress component $\mathcal{T}_{12}$, as shown in Fig. 2(d), is zero and $\mathcal{T}_{13}\sim\pm0.5$ GPa at the interface, [see Fig. 2(e)]. We thus proved that an epitaxial film, which is not lattice matched to its substrate, will be under uniform biaxial contraction ($\varepsilon_\parallel<0$) or dilatation ($\varepsilon_\parallel>0$), in the plane of film. The in-plane strain $\varepsilon_\parallel$ is given by the substrate and layer material bulk lattice constants, thus, $\varepsilon_{11}=\varepsilon_{22}=\varepsilon_\parallel=a_{\mathrm{AlGaAs}}/a_{\mathrm{GaAs}}-1$ and $\varepsilon_{12}=0$, where a_{AlGaAs} and a_{GaAs} are, respectively, the lattice parameter of barrier and well materials. Therefore, three strain tensor components must be determined: ε_{13}, ε_{23}, and $\varepsilon_{33}=\varepsilon_\perp$. There is no in-plane shear strain in the film under uniform biaxial distortion (in-plane angles between ions are preserved).[21,22] This allows the representation of the strain components for a system grown along the direction [113] given by $\varepsilon_\perp=-\frac{198\mathcal{C}_{11}^2-45\mathcal{C}_{11}\mathcal{C}_{12}-374\mathcal{C}_{11}\mathcal{C}_{44}-153\mathcal{C}_{12}^2+1245\mathcal{C}_{12}\mathcal{C}_{44}-44\mathcal{C}_{44}^2}{11(9\mathcal{C}_{11}^2+9\mathcal{C}_{11}\mathcal{C}_{12}+9\mathcal{C}_{11}\mathcal{C}_{44}-18\mathcal{C}_{12}^2-34\mathcal{C}_{12}\mathcal{C}_{44}+4\mathcal{C}_{44}^2)}\varepsilon_\parallel$ and $\varepsilon_{13}=-\frac{12\sqrt{2}(11\mathcal{C}_{11}^2+2\mathcal{C}_{11}\mathcal{C}_{12}-22\mathcal{C}_{11}\mathcal{C}_{44}-13\mathcal{C}_{12}^2-26\mathcal{C}_{12}\mathcal{C}_{44})}{11(9\mathcal{C}_{11}^2+9\mathcal{C}_{11}\mathcal{C}_{12}+9\mathcal{C}_{11}\mathcal{C}_{44}-18\mathcal{C}_{12}^2-34\mathcal{C}_{12}\mathcal{C}_{44}+4\mathcal{C}_{44}^2)}\varepsilon_\parallel$, where $\mathcal{C}_{11}$, $\mathcal{C}_{12}$, and $\mathcal{C}_{44}$ are elastic constants of the material (in our case $\varepsilon_\perp=-0.4074\cdot\varepsilon_\parallel$ and $\varepsilon_{13}=0.2248\cdot\varepsilon_\parallel$). It is remarkable the complexity of matrix elements for Luttinger, Bir-Pikus Hamiltonian, and for the strain tensor components along

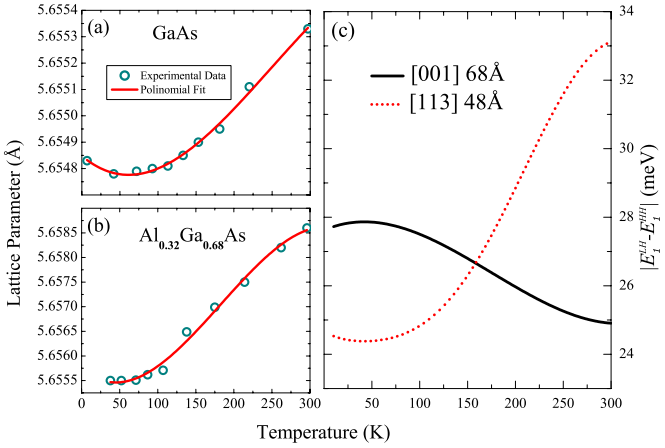

FIG. 3. (Color online) Temperature dependence of the lattice parameter for (a) GaAs and (b) $Al_{0.32}Ga_{0.68}As$. The experimental data were fitted with a third-degree polynomial. (c) Temperature dependence of the difference between LH and HH energy peaks, $|E_1^{\mathrm{LH}}-E_1^{\mathrm{HH}}|$, along [001] and [113] directions for different configurations of well widths [that fit the absolute positions of the HH transition energies in Figs. 1(a) and 1(b)].

[113] direction if we compare them with those along [001] direction, where the relation between strain components reduces simply to $\varepsilon_\perp=-(\frac{2\mathcal{C}_{12}}{\mathcal{C}_{11}})\varepsilon_\parallel$ (Ref. 13) (that corresponds to $\varepsilon_\perp=-0.9279\cdot\varepsilon_\parallel$ in the case under consideration).

Given the analytical expressions described above, along with the values of the stress tensor components, we can solve the eigenvalue problem for the total Hamiltonian. For the calculations we used the following Luttinger parameters:[23] $\gamma_1=6.85$, $\gamma_2=2.10$, and $\gamma_3=2.90$. For the deformation potential, we have used the following values:[24] $a=2700$, $b=-1700$, and $d=-4550$. For the elastic constants, we have used the following values:[25] $\mathcal{C}_{11}=122.1$ GPa, $\mathcal{C}_{12}=56.6$ GPa, and $\mathcal{C}_{44}=59.9$ GPa. The main contrasting behavior between systems grown along the directions [001] and [113] is the opposite slope of the difference between LH and HH energy peaks with temperature and with strain increase. It is interesting to note that the diagonal terms in the Bir-Pikus Hamiltonian, that determine the intersubband splitting in the valence band for the system grown along [001] direction, $P_{BP}^{+}-P_{BP}^{-}=-5.79\cdot\varepsilon_\parallel$ eV, do not act as the main factors in the [113] case. Here, the difference between diagonal terms yields $P_{BP}^{+}-P_{BP}^{-}=-5.19\cdot\varepsilon_\parallel$ eV, with the same sign as in the system grown on the (001) plane. Thus, the positive slope comes from contributions of the nondiagonal terms that couple the HH and LH subbands.

To express the temperature dependence of $\varepsilon_\parallel$, the lattice-parameter dependence on temperature must be used as shown in Fig. 3, for GaAs (Ref. 26) and AlGaAs.[27] In order to obtain a functional dependence, we fitted the experimental points with a third-order polynomial $a(T)=a_0+a_1T+a_2T^2+a_3T^3$, as shown in Figs. 3(a) and 3(b). From the experimental data of the lattice-parameter dependence with temperature, we can estimate the variation in strain due to changes in the lattice parameters within the range $0.012<\varepsilon_\parallel<0.058$. A slight variation in the lattice parameter produces large variation in the band structure of the system. In Figs. 3(a) and

3(b), it is possible to see how small is the variation in the lattice parameter for the given temperature range. Figure 3(c) shows the temperature dependence of the absolute difference between LH and HH energies for [001] and [113] directions. If we compare Figs. 1(c) and 3(c), we can see that the theoretical model describes correctly the experimental behavior.

In summary, the variation in strain conditions with temperature has revealed the contrasting optical responses of layered systems grown in the directions [001] and [113]. Experiments demonstrate differences in the dependence of the valence-subband splitting between the HH and LH bands depending on growth direction. This behavior has been supported by the multiband calculation for the respective electronic structure. The molecular-dynamics simulation revealed the nature of strain fields by showing the behavior of the stress tensor components. The external control of the valence-subband splitting between HH and LH, either by temperature or stress, may be used to tune the intersubband coupling by LO phonons. This process is allowed by hole-phonon deformation-potential interaction.[28] The resonant condition for this interaction depends on the match between the LO-phonon energy [$\hbar\omega_{LO}$=37 meV (Ref. 29)] and the HH-LH energy subband separation. According to Figs. 1(c) and 3(c), the energy splitting of the sample grown along [113] direction displays values above 30 meV (which can also be tuned by reducing the well width). This analysis can be extended for nanostructures, such as wires and quantum dots. Recently, the use of HH-LH subband separation (by controlling strain fields) has been proposed for optical applications of nanoscopic wires.[30,31]

[1] O. Brandt, K. Kanamoto, Y. Tokuda, N. Tsukada, O. Wada, and J. Tanimura, Phys. Rev. B **48**, 17599 (1993).
[2] J. B. Xia, Phys. Rev. B **43**, 9856 (1991).
[3] E. P. O'Reilly, Semicond. Sci. Technol. **4**, 121 (1989).
[4] Calvin Yi-Ping Chao and S. L. Chuang, Phys. Rev. B **46**, 4110 (1992).
[5] J. A. Porto and J. Sanchez-Dehesa, Phys. Rev. B **51**, 14352 (1995).
[6] M. P. Houng, Y. C. Chang, and W. I. Wang, J. Appl. Phys. **64**, 4609 (1988).
[7] N. Galbiati, E. Grilli, M. Guzzi, M. Henini, and L. Pavesi, Microelectron. J. **28**, 993 (1997).
[8] V. Lopez-Richard, G.-Q. Hai, C. Trallero-Giner, and G. E. Marques, Phys. Rev. B **66**, 155303 (2002).
[9] V. López-Richard, G.-Q. Hai, C. Trallero-Giner, and G. Marques, Phys. Rev. B **67**, 155320 (2003).
[10] M. D. Teodoro, I. F. L. Dias, E. Laureto, J. L. Duarte, P. P. González-Borrero, S. A. Lourenço, I. Mazzaro, E. Marega, Jr., and G. J. Salamo, J. Appl. Phys. **103**, 093508 (2008).
[11] S. A. Lourenço, I. F. L. Dias, E. Laureto, J. L. Duarte, D. O. Togino Filho, E. A. Meneses, and J. R. Leite, Eur. Phys. J. B **21**, 11 (2001).
[12] S. L. S. Freire, J. E. T. Reis, L. A. Cury, F. M. Matinaga, J. F. Sampaio, and F. E. G. Guimarães, Phys. Rev. B **64**, 195325 (2001).
[13] G. Fishman, Phys. Rev. B **52**, 11132 (1995).
[14] R. Winkler and A. I. Nesvizhskii, Phys. Rev. B **53**, 9984 (1996).
[15] R. Andr, Ph.D. thesis, University J. Fourier-Grenoble 1, 1994.
[16] G. E. Pikus and G. L. Bir, Sov. Phys. Solid State **1**, 136 (1959).
[17] I. Vurgaftman, J. R. Meyer, and L. R. Ram-Mohan, J. Appl. Phys. **89**, 5815 (2001).
[18] P. S. Branicio, J. P. Rino, F. Shimojo, R. K. Kalia, A. Nakano, and P. Vashishta, J. Appl. Phys. **94**, 3840 (2003).
[19] D. W. Brenner, Phys. Status Solidi B **217**, 23 (2000); and M. Z. Bazant, E. Kaxiras, and J. F. Justo, Phys. Rev. B **56**, 8542 (1997).
[20] P. Branicio and D. J. Srolovitz, J. Comput. Phys. **228**, 8467 (2009).
[21] J. M. Hinckley and J. Singh, Phys. Rev. B **42**, 3546 (1990).
[22] H. Mathieu, P. Lefebvre, and P. Christol, Phys. Rev. B **46**, 4092 (1992).
[23] K. Hess *et al.*, *Physics of Semiconductors: Proceedings of the 13th International Conference* (North-Holland, New York, 1976), p. 142.
[24] S. Adachi, J. Appl. Phys. **58**, R1 (1985).
[25] *Comprehensive Index*, Landölt-Börnstein, New Series, edited by O. Madelung and W. Martienssen (Springer, Berlin, 1996).
[26] G. Clec'h, G. Calvarin, P. Auvray, and M. Baudet, J. Appl. Crystallogr. **22**, 372 (1989).
[27] M. Leszczynski, V. B. Pluzhnikov, A. Czopnik, J. Bak-Misiuk, and T. Slupinsk, J. Appl. Phys. **82**, 4678 (1997).
[28] V. Lopez, G. E. Marques, J. Drake, and C. Trallero-Giner, Phys. Rev. B **56**, 15691 (1997).
[29] V. Lopez-Richard, G. E. Marques, C. Trallero-Giner, and J. Drake, Phys. Rev. B **58**, 16136 (1998).
[30] V. López-Richard, J. C. Gonzalez, F. M. Matinaga, C. Trallero-Giner, E. Ribeiro, M. Rebello Sousa Dias, L. Villegas-Lelovsky, and G. E. Marques, Nano Lett. **9**, 3129 (2009).
[31] M. Montazeri, M. Fickenscher, L. M. Smith, H. E. Jackson, J. Yarrison-Rice, J. H. Kang, Q. Gao, H. Hoe Tan, C. Jagadish, Y. Guo, J. Zou, M.-E. Pistol, and C. E. Pryor, Nano Lett. **10**, 880 (2010).